photonics

MDPI

Article

A Novel Design of Optical Switch Based on Guided Mode Resonances in Dielectric Photonic Crystal Structures

Atiq Ur Rehman [1], Yousuf Khan [1,*], Muhammad Irfan [1], Muhammad A. Butt [2,3], Svetlana N. Khonina [3,4] and Nikolay L. Kazanskiy [3,4]

[1] Nanophotonics Research Group, Department of Electronic Engineering, Balochistan University of Information Technology, Engineering and Management Sciences, Quetta 87300, Pakistan
[2] Institute of Microelectronics and Optoelectronics, Warsaw University of Technology, Koszykowa 75, 00-662 Warszawa, Poland
[3] Samara National Research University, 443086 Samara, Russia
[4] Image Processing Systems Institute of RAS—Branch of the FSRC "Crystallography and Photonics" RAS, 443001 Samara, Russia
* Correspondence: yousuf.khan@buitms.edu.pk

Abstract: In this work, a novel idea of optical switch design based on guided mode resonance in the photonic crystal structure is numerically investigated. The designed switching device work on the principle of optical amplification and wavelength shift of data signal with the help of a control signal. The data signal can be coupled into the waveguide using guided-mode resonance, whereas, a control signal is index-coupled into the waveguide to influence the data signal. The optical switching action is optimized by introducing a photonic crystal cavity and varying the number of photonic crystal elements, where the resonant wavelength, reflection peaks, linewidth, and quality factor of the data signal can be adjusted. The device is based on low refractive index contrast dielectric materials compatible with fiber optic communication and can operate in a near-infrared range of around 1.55 µm. The numerical simulations are carried out in an open source finite-difference time-domain-based software. An optical switching action is achieved with 7% amplification in the data signal at a central wavelength of 1.55 µm with a maximum shift of the wavelength of 0.001 µm. The proposed device can be easily implemented in cascade designs of programmable photonic and optical switching circuits.

Keywords: optical switch; optical switching circuits; photonic crystals; finite difference time domain; guided mode resonances

Citation: Rehman, A.U.; Khan, Y.; Irfan, M.; Butt, M.A.; Khonina, S.N.; Kazanskiy, N.L. A Novel Design of Optical Switch Based on Guided Mode Resonances in Dielectric Photonic Crystal Structures. *Photonics* **2022**, *9*, 580. https://doi.org/10.3390/photonics9080580

Received: 19 July 2022
Accepted: 14 August 2022
Published: 17 August 2022

1. Introduction

With the advancement in modern technology and the introduction of artificial intelligence, the need for faster and high-performance computing is on the rise. Electronic technology has already reached its limits in terms of speed, performance, and power efficiency. Moreover, the current technology makes use of fiber optics for long-haul communication and electronic technology for information processing, which limits the processing and power efficiency of the system. To address these limitations, scientists are exploring new frontiers for the optical processing of information such as photonic computing [1]. Photonic computing has already been proposed for human brain-like computing [2], programable photonic circuits [3] and photonic integrated circuits [4]. Keeping in mind the basic building block for electronic logic flow, the electronic transistor, different techniques to implement optical switching or optical transistor action have been under consideration such as ring resonators [5], cross-waveguide structures [6], optical pumping [7], hybrid electro-optical devices [8,9] and quantum dots [10]. Most of the device structures in the suggested techniques are complex to implement in large quantities such as in design and

fabrication of a photonic integrated circuit [11]. An easy-to-implement and compact design to make an optical switching device is to make use of the Guided-mode resonance (GMR) also known as the Fano-resonance [12], a phenomenon in two-dimensional Photonic Crystals (PhCs) structures which works on the principle of out-of-the-plane coupling of light in the structures. During GMR, the free-space modes in the incident light interfere with the leaks modes and the guided modes inside the structures using phase matching mechanism to create resonances. PhCs are capable of guiding and manuplating the light at wavelength scale [13] and their usage has been reported in various optical filtering [14] and sensing [15,16] applications. This work presents a novel idea to implement optical switching action using optical amplification in PhC structures by enabling interference of in-plane index-guided modes and out-of-the-plane coupled resonances.

Optical switching action is proposed using different techniques including a cross-waveguide geometry [6], Fano resonances-based structures [17], spontaneous generated coherence (SGC) [18], and plasmons-induced enhancement of index of refraction [19]. A defect mode design using PhCs to implement the optical switching phenomenon is presented in [20]. Equally, a method to implement optical switching using the PhCs waveguides and cavities is suggested in [21]. Whereas, refs. [22,23] investigate a photonic bandgap microcavity-based design for optical switching. PhCs-based directional couplers are also reported for optical switching by varying the refractive index contrast of the materials using numerical simulations in Plane Wave Expansion (PWE) and Finite Difference Time Domain (FDTD) domains [24]. The integration of the passive silicon (Si) PhCs-based waveguide and the active III-V materials to reduce the coupling losses during the switching process is presented in [25]. Similarly, Ref. [26] makes use of PhC-based point defect and line-defect waveguide structures to investigate optical switching. The plasmonic property of the materials is also explored in [27] to design an efficient optical switch using the ultrafast light-matter interaction property of the plasmons. Similarly, a ring resonator-based design using graphene and Si rods between two waveguides is studied using the PWE method in [28,29] to produce the characteristics of optical switching. Another structure of the Erbium-doped fiber amplifier model is used for the design of the optical switch for long-haul communication systems [30]. A design of the optical switch is presented in [31] using the artificial epsilon-near-zero approach in metal-insulator-metal to cause the phenomenon of reflectance at ultrafast speed. Moreover, Ref. [32] employs quantum dots, where a primary signal is controlled with the help of another weak pump signal imitating the idea of optical switching and [33] studies interference of two signals by GMR and total internal reflection in PhCs to investigate optical switching. Moreover, PhC-based optical logic gates have also been an exclusive topic of research nowadays. PhC waveguide-based modulators [34], all half adder, XOR, and AND gates using 2D PhC structure have been presented in [35–38]. However, no research has been reported on a dual device implementing optical switching and filtering of signal using GMR in 2D PhC structures.

This work numerically investigates all-optical switching actions for near-infrared communication. The switching mechanism is implemented in 2D PhC structure, where an out-of-the-plane coupled data signal is amplified with an index-guided control signal. Moreover, presents a novel concept in terms of bringing the out-of-the-plane and index-guided signals together, which investigates an easy-to-implement optical switch design. Apart, from these, it offers the advantage to be used in different optical components i.e., optical filters, transistors, modulators, and logic gates [39]. The symmetric condition of the arrangement is another advantage of the research, as the change in the radius of the cavity, will bring a considerable change in the tunning of the GMR modes rather than having cavities on both sides of the structure as compared to the already presented investigation in [40]. A conceptual diagram representing the basic working of the optical switching device integrated into the photonic logic circuit is shown in Figure 1a, where a 4-bit bus carrying a data signal is optically switched using 4-bit control signals. A low-index contrast dielectric material-based slab-waveguide PhC structure is used to make the device compatible with fiber optic communication. A waveguide material based on Niobium pentaoxide (Nb_2O_5)

is deposited on a silicon dioxide (SiO_2) glass substrate as an optical membrane and covered with a SiO_2 cladding layer as presented in Figure 1b. The refractive indices of Nb_2O_5 and SiO_2 for the NIR range are implemented as n_w = 2.2 and n_s = 1.5 respectively, which are taken as a reference from experimental results presented in [12,41]. The optical switching action is optimized by varying the size and position of the PhC nano-cavity and the number of PhC-elements. The proposed investigation presents a cost-effective, compact, and easy-to-fabricate device based on dielectric materials suitable for a broad spectral range, unlike semiconductor material based devices investigated in [4,10,19,24], which can have limitations being bulky, expensive and difficult to fabricate designs.

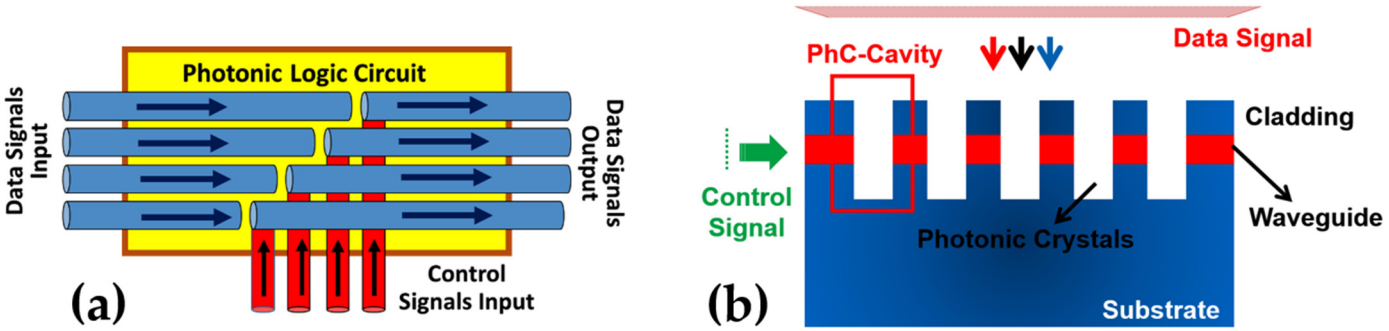

Figure 1. (**a**) Conceptual design of the optical switches in a photonic logic circuit (**b**) Schematic of the designed optical switch.

2. Simulation Approach

The optical switching action is investigated using 2D-FDTD simulations in an open-source software platform, the so-called MIT Electromagnetic Equation Propagation (MEEP) [42,43]. The time-domain simulations in MEEP compute the electric and magnetic fields by solving Maxwell's equations [41]. The FDTD offers the advantage to use a short Gaussian pulse to compute the response of the system over a wide frequency range. The pictorial representation of the simulation domain is shown in Figure 2a where the multilayer structure with a waveguide layer submerged between the substrate and cladding layer can be seen. A plane-wave source above the structure indicates the data signal, which is coupled into the PhC structure, where it is filtered by GMR. To implement the optical switching mechanism, a control signal (shown on the left) is index-coupled into the waveguide. The date signal is monitored above and below the waveguide as reflection and transmission flux as indicated in the figure. The simulation cell is terminated using Perfectly Matched Layer (PML) boundary conditions to absorb all the outgoing EM fields in both X and Z-directions. While Figure 2b presents the real investigated structure comprising of a variable PhC-cavity at the start of the structure. Figure 2c is the zoomed image of the PhC-cavity, showing its geometrical parameters in terms of radius, depth of the PhC-hole and thickness of the cladding layer. Moreover, the radius of the PhC-cavity is varied to investigate its effects on the resonant wavelength in cylinderical PhC-elements. However, since this work is based on 2D-FDTD simulations, the shape of these air-hole based PhC-elements appear to be rectangular gratings.

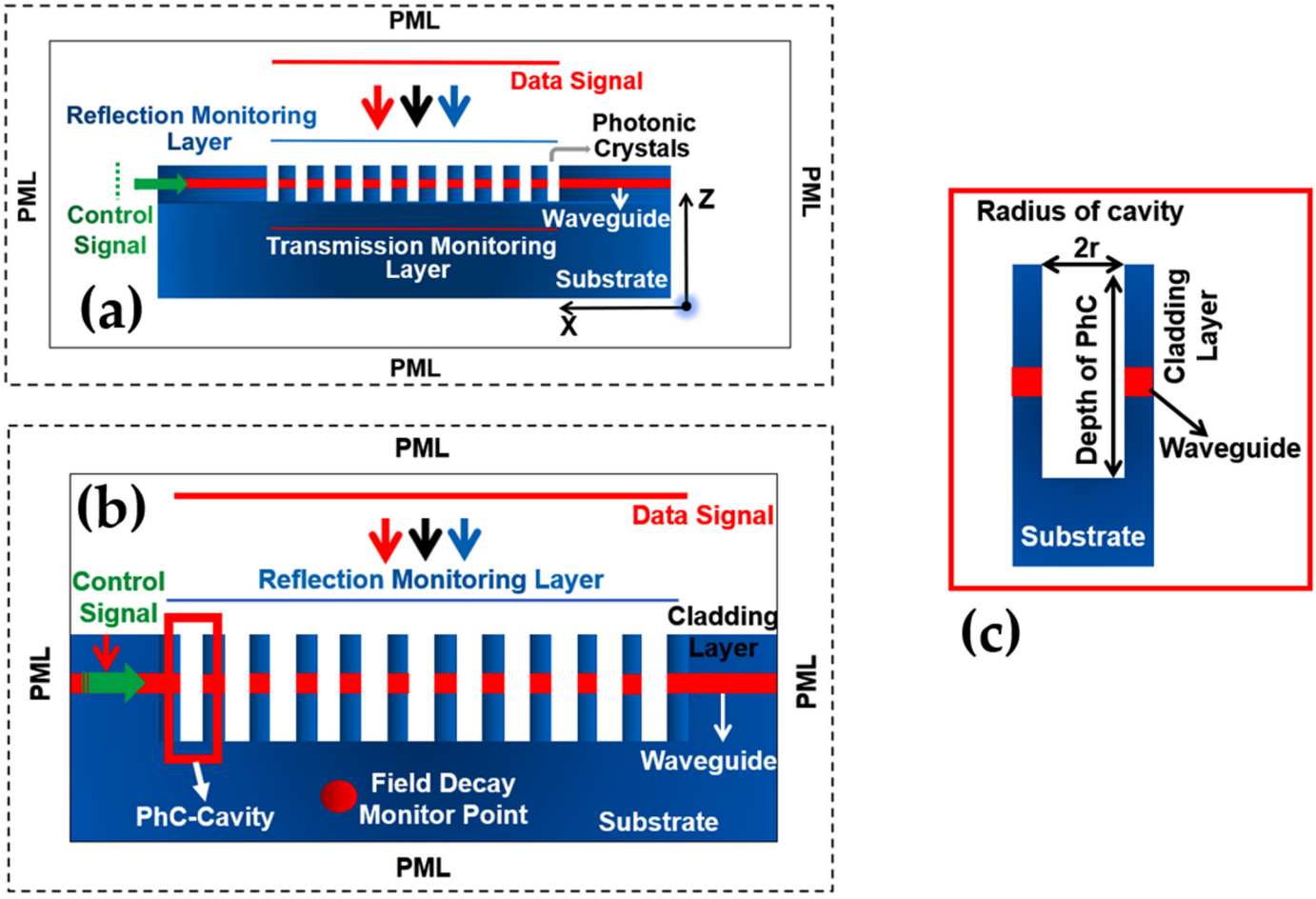

Figure 2. (**a**) Basic simulation model showing the position of the data signal, control signal, boundary condition, and field monitoring layers (**b**) Real investigated structure (**c**) Zoom image of the PhC-cavity.

3. Designing Parameters

To enable the device to operate in NIR telecommunication range around 1.55 µm, the lattice constant was designed to be a = 1 µm. All other design parameters are mentioned in terms of lattice constant to enable rescaling of the device to a different wavelength range. Moreover, the depth of the PhC elements is kept constant as 1.8a. The optimized values of the structural design parameters of the proposed device are summarized in Table 1 and depicted in Figure 3.

Table 1. Optimized design parameters of the proposed optical switching device.

Parameters	Symbol	Value
Lattice constant	a	1 µm
Radius of the PhC-elements	r	0.207a
Thickness of waveguide	w	0.44a
Thickness of cladding	-	0.68a
Refractive index of the substrate	SiO_2	$n_s = 1.5,\ \varepsilon = 2.25$
Refractive index of the waveguide	-	$n_w = 2.2,\ \varepsilon = 4.84$
Resonant wavelength	ω_c	1.55 µm
Thickness of PML layer	PML	3.0a

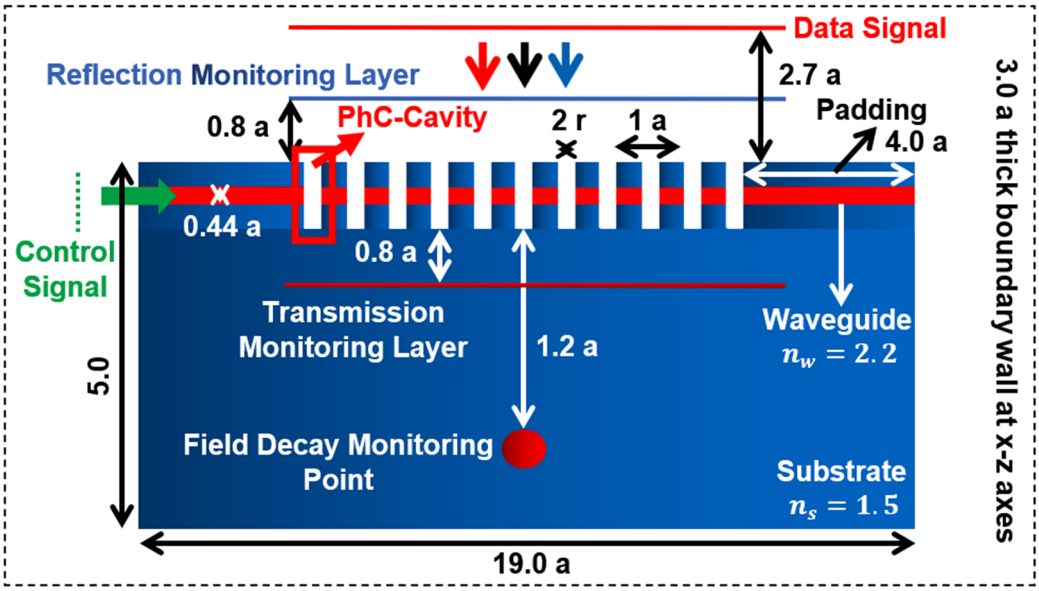

Figure 3. The structure of the optical switch reflecting the details of the parameters used.

The data signal is defined as a Gaussian time profile source placed at a distance of 2.70*a* above the structure. Similarly, the control signal having the same spectral properties is placed at the start of the waveguide to enable index coupling of fields. Moreover, the pulse response of the system is computed for a user-defined number of frequency points for both of the sources as n_f = 550. The transmission and reflection monitoring layers are placed at a distance of 0.8*a* below and above the structure respectively. Similarly, the field decay monitor point monitors the field decay at a user-defined point in the domain with a user-defined value of field intensity, where the simulation should terminate. To ensure accurate and good-quality computational results, the grid size of the simulation domain must be smaller than the smallest wavelength in the EM spectrum of the excitation sources. A grid resolution value of 20 is used with a smoothing factor of 0.05, which is smaller than wavelength/30 equaling a grid size of 0.052.

4. Results

In the first step, the design parameters of the device were optimized to achieve a reflection peak with resonance at a central wavelength of ω_c = 1.55 µm. The design parameters to be optimized include the thickness of the waveguide and cladding layer, radius, depth of the air-holes, number of PhC-elements, and radius of the PhC-cavity. Moreover, the spectral properties of the excitation sources also need to be optimized, which include central wavelength, bandwidth, size and positions of the data, and control signal. The optimized value of the mentioned parameters is given in Table 1 and the spectral response of the device against these parameters with just the data signal is shown in Figure 4. The transmission and reflection spectrum shows a resonant peak at ω_c = 1.55 µm and reflection peak of 70% with 11 periods of PhC-elements and without the presence of a cavity. This spectral result is used as a reference and the investigation of the effect of all other design parameters on the spectral response as presented in upcoming the subsections. In the first step, the investigations are carried out for a single source (data signal) and later optical switching action is investigated with two sources (data and control signal simultaneously).

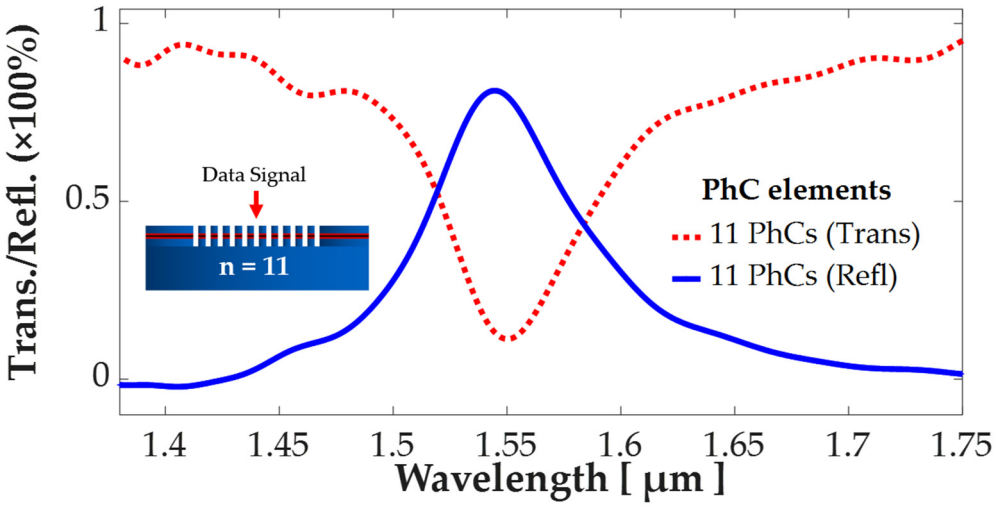

Figure 4. Transmission and reflection spectra of an 11 PhCs-based structure.

4.1. Effect of the Number of PhC Elements on A Data Signal

The number of the PhC elements is an important aspect of the investigation, as it affects the coupling of energy into the optical membrane and the effects of the control signal on the data signal to perform the optical switching. Therefore, in this analysis, the number of PhCs varied from 9 to 15 with an increase of 2 elements as shown in Figure 5 (reflection spectrum), simulated by a data signal. It can be seen that as the number of the PhC-elements increase, the energy of the resonant mode becomes stronger, and hence the reflection peak rises. The reflection peak at the ω_c is 60% for 9 PhC-elements and it increases up to 79% for 15 PhC elements. As R represents the reflection peak, the resonances characteristics of Figure 5, are calculated and presented in Table 2, by using the following equations.

$$\text{Reflection (R)} = R_{max} - R_{min} \tag{1}$$

$$\text{Finesse (F)} = \frac{\pi\sqrt{R}}{1-R} \tag{2}$$

$$\text{Linewidth} = \frac{FSR}{Finesse} \tag{3}$$

$$\text{Free Spectral Range (FSR)} = Finesse \times Linewidth \tag{4}$$

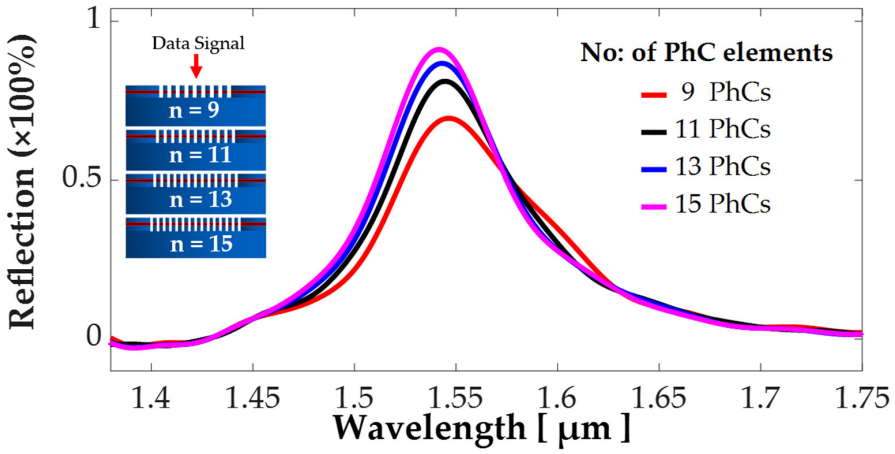

Figure 5. The reflection spectrum of PhC structure for variation in the number of periods of PhC-elements for the data signal.

Table 2. Resonance characteristics of structures based on 9, 11, 13, and 15 PhC periods using data signal.

Number of PhCs Periods	Single Source (Data Signal)			
	Reflection %	**Finesse**	**Linewidth (μm)**	**FSR (μm)**
09 PhC-elements	60	6.08	0.073	0.444
11 PhC-elements	70	8.763	0.07	0.613
13 PhC-elements	71	9.129	0.066	0.603
15 PhC-elements	79	13.298	0.061	0.811

From Table 2 it can be assessed that as the number of PhC elements increases, the confinement of optical energy increases, increasing the percentage of the reflection peak at ω_c. Whereas, the value of F increases and the linewidth decreases improving the optical filtering mechanism. Thus, it is preferable to have a higher number of PhC elements in the structures for single soure operation. However, it was also found that a larger number of PhC-elements decreases the effects of the control signal on the output of the data signal. This is because by increasing the number of the PhCs, there is a change in the effective refractive index of the waveguide and more accumulation of the air within the structure. Hence, this affects the efficiency of the control signal to bring a significant amplification in the output of the data signal. Moreover, it acts as analogous to the depletion region in the electronic transistor, where the transistor act as an open switch when the depletion region is large enough and when the base signal is applied, the depletion region narrows and transistor acts as a closed switch. Therefore, this investigation was limited to 15 PhC-elements and as a result, the unity figure for the summation of the transmission and reflection spectrums is comprised.

4.2. Effect of the Radius of PhC-Cavity with A Data Signal

To investigate the optical amplification and switching mechanism, a PhC cavity is placed at the start of the structure. Initially, the radius of the PhC cavity is varied for different periods of PhC elements to study its effect on the data signal. The radius of the cavity is varied from $r_c = 0.06a - 0.35a$ for the number of PhC-elements as 9, 11, 13, and 15 in reflection spectra as shown in Figure 6, with an inset showing the zoomed image of the difference between the peaks.

The variation in the radius of the PhC cavity at the start of the membrane shifts the ω_c to a noticeable range. As the radius of the cavity increases, ω_c undergoes a blueshift and vice versa. This the because the drop in fill factor results in a decrease in the effective refractive index of the periodic waveguide and a drop in the coupling of the energy into the membrane. Similarly, when the radius of the cavity is slightly lower i.e., $0.150a$ as compared to the radius of the PhC elements used in the arrangement i.e., $0.207a$, the quality of the spectrum is maximum in terms of reflection peak and linewidth. Correspondingly, by increasing the radius of the cavity further to $0.35a$, the ω_c undergoes a redshift and the coupling of energy starts to decrease abruptly. Figure 6a depicts output spectra of the 9 PhCs-based structure with varying cavity-radius for data signal, where the reflection peaks are lowest as compared to other cases. Whereas, Figure 6b depicts the reflection spectra for 11 PhC periods showing an increase in the values of the reflection peaks and coupling of energy into the optical membrane. Figure 6c shows an increase in the reflection peak values where the radius of cavity is varied for 13 periods of PhCs. Figure 6d displays the highest values of the reflection peaks for cavity-radius variation in 15 periods of PhCs. Additionally, the position of the cavity was checked on both lateral ends of the membrane which yielded the same results.

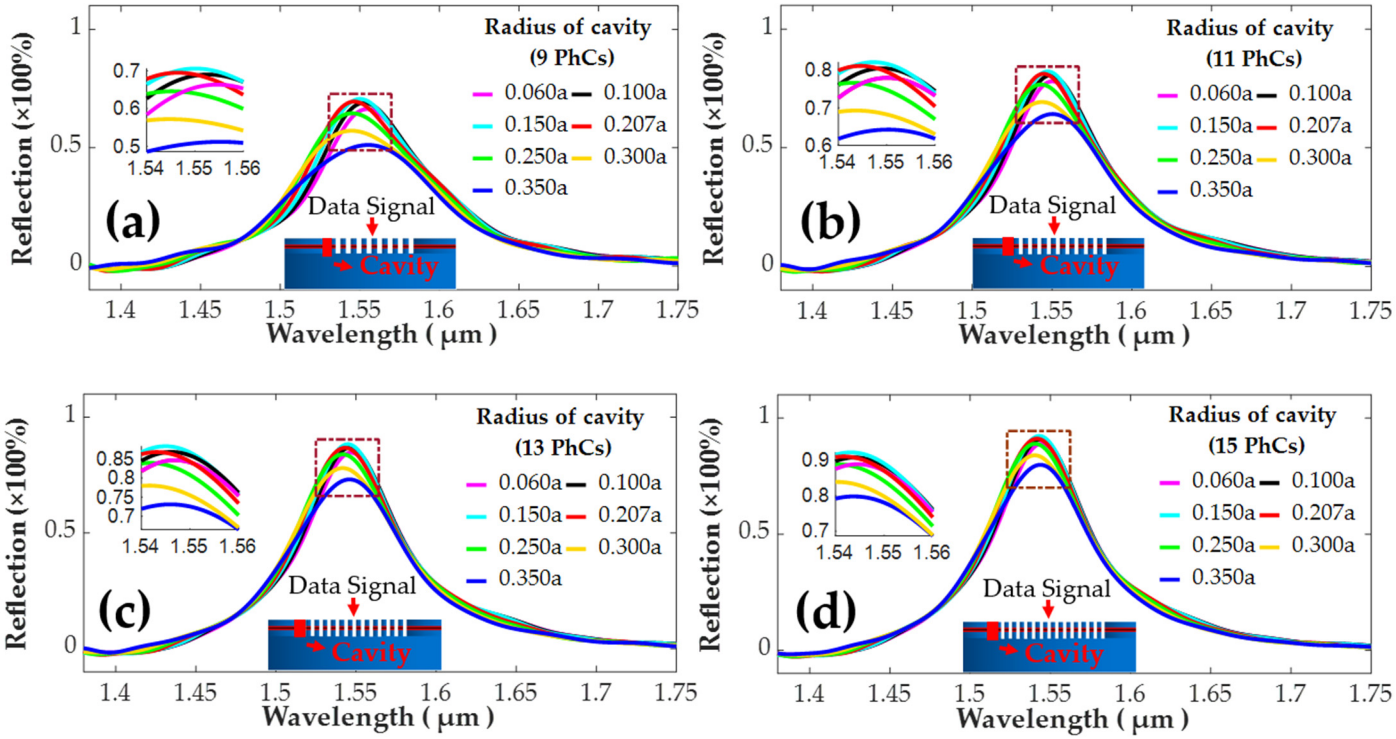

Figure 6. Effects of radius of PhC-cavity on the reflection peaks for (**a**) 9 PhC-elements (**b**) 11 PhC-elements (**c**) 13 PhC-elements (**d**) 15 PhC-elements.

4.3. Comparative Analysis of Spectral Properties for Variation in the Number of PhC-Elements and Radius of PhC-Cavity for Data Source

A detailed analysis of spectral properties for variation in cavity radius in stuctures with number of PhC elements as 9, 11, 13 and 15 is shown in Figure 7. Where Figure 7a depicts the variation in reflection peaks and shifting of ω_c as the radius of the cavity is changed. The graphical trends depict a maximum variation in reflection peaks and shifts in ω_c for 9 PhC element-based structure. Whereas, the maximum values of reflection peak are achieved for 15 PhC elements. Similarly, Figure 7b plots linewidth of resonant modes against the cavity-radius in order to determine the optimum value of cavity-radius to get the best quality of the data signal. Wherein, the structure with 9 PhCs, presents the highest values of linewidth which means a lower optical filtering characteristics and confinement of energy into the structure. Furthermore, as the number of the PhCs increases, the linewidth reduces depicting better confinement of guided modes. Figure 7c shows the variation in reflection peaks with respect to the variation in the cavity radius. It can be seen that as the cavity radius increases, the reflection drops which corresponds to drop in the effective refractive index of the periodic structure. Figure 7d, displays the electromagnetic (EM) field distribution for two different cavity radii of r = 0.06*a* and r = 0.35*a* in a 11 PhC structure, where the variation in the localization of resonant modes can be observed.

4.4. Analysis of the Quality Factor for the Variation in the Number of PhC-Elements and Radius of PhC-Cavity for Data Source

The quality factor of resonant modes for a varying number of PhC-elements is shown in Figure 8. The quality factor is calculated for cavity-radius in the range of r = 0.06*a* to 0.35*a* for 9 to 15 PhC-elements. It can be observed that the highest quality factor is achieved for 15 PhC-element-based structures regardless of the cavity-radius selection, which indicates a better field coupling and confinement in larger number of PhC-elements. Moreover, it can be seen that the quality factor is highest for cavity-radius value of r = 0.15*a* in all the cases ranging from 9 to 15 PhC-elements. It drops rapidly as the cavity-radius

exceeds r = 0.15*a*. The reason can be explained as the drop in fill-factor as the radius of the PhC-elements increases which results in a drop in the value of the effective refractive index of the waveguide.

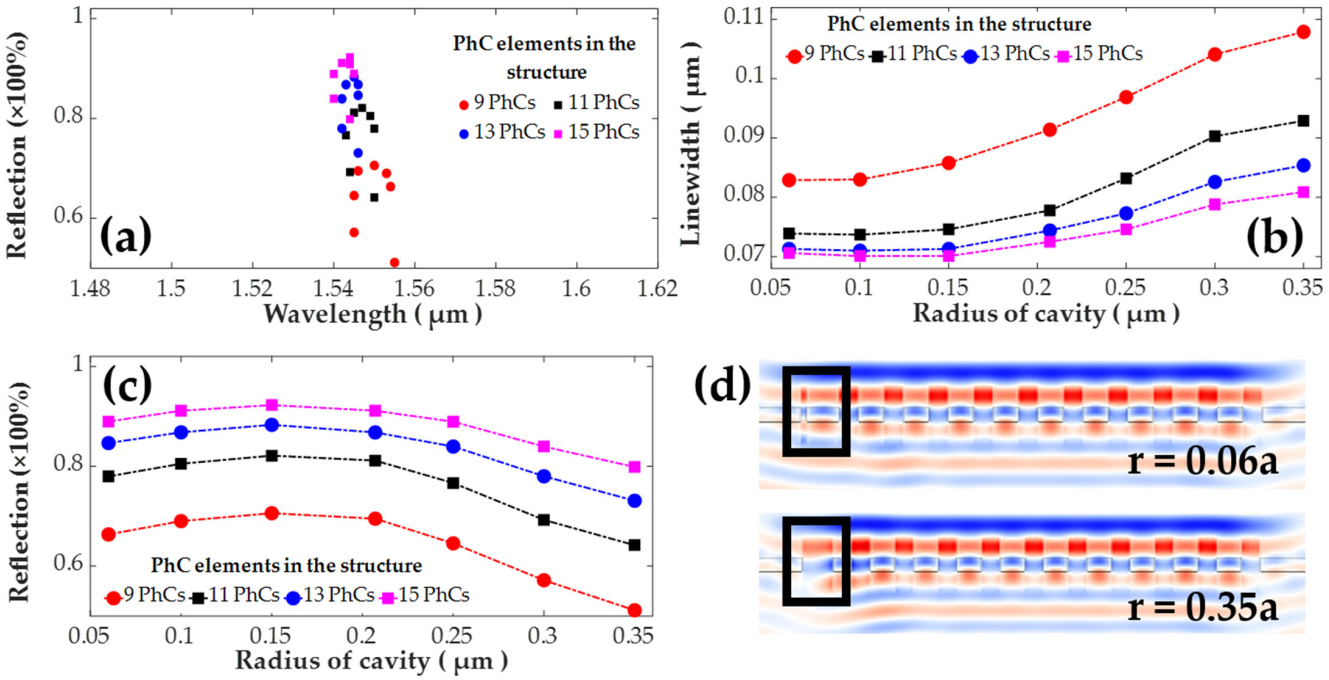

Figure 7. Analysis of spectral properties of PhC structures for variation in number of PhCs and cavity-radius. (**a**) Reflection vs wavelength. (**b**) Linewidth vs cavity-radius. (**c**) Reflection vs. cavity-radius. (**d**) EM field distribution for cavity-radii as r = 0.06*a* and 0.35*a*.

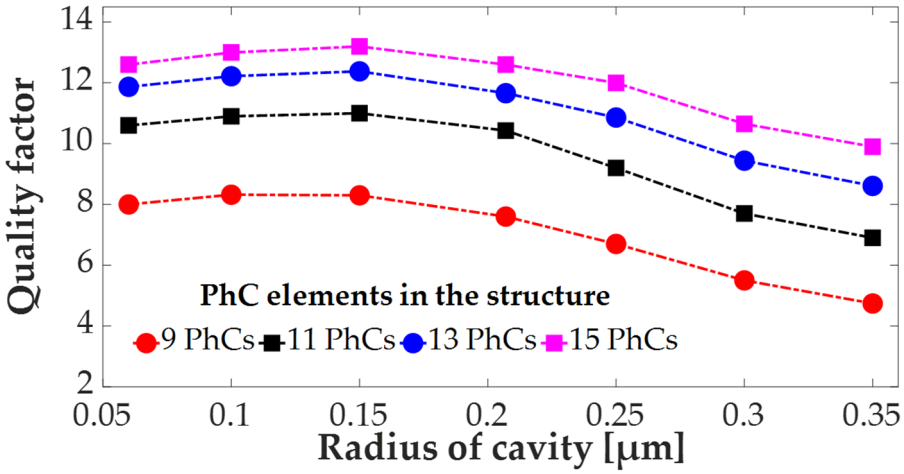

Figure 8. The quality factor of PhC structure for variation in the number of PhC-elements and PhC cavity-radius for the data signal.

4.5. Transistor Action in Different PhCs Structures Using Both the Signals (Data and Control)

After investigating the effects of the cavity-radius and number of PhC-elements on spectral properties of the device using a data signal, the next step is to implement the control signal to study the optical switching action. The goal is to choose the values of structural design parameters in such a way that the control signal must interference and significantly amplify a weak data signal to perform an optical switching action. The reflection spectra for variation in cavity-radius for different numbers of PhC-elements using both data and control signal are shown in Figure 9. To visualize the optical amplification, the reflection

spectra for the data signal is plotted with a solid line, whereas, the reflection spectra for both data and control signal is plotted with a dotted line. Insets in the Figure 9a–d show a zoomed view of the reflection peaks.

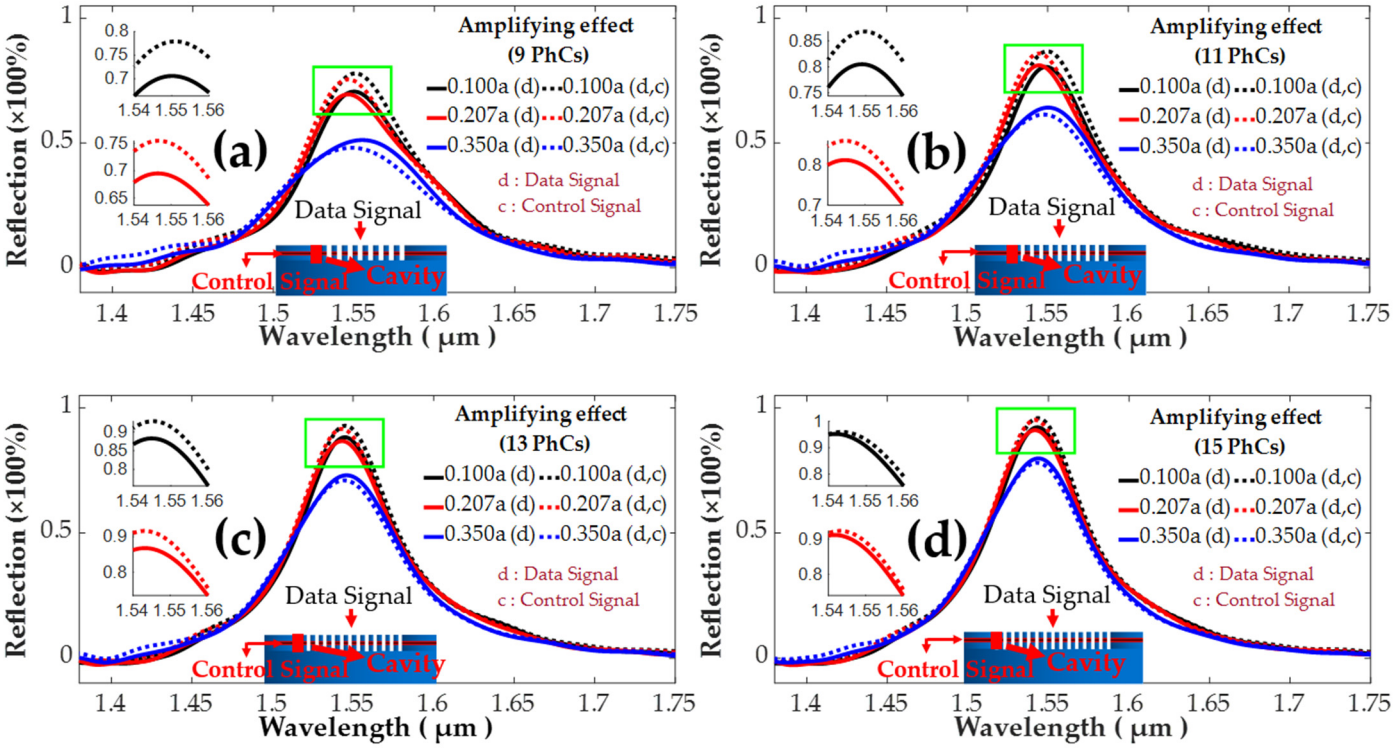

Figure 9. Reflection spectra of PhC structures for both data and control signal to investigate optical amplification and switching action. The cavity-radius is varied for a case study in different number of PhC-elements. (**a**) 9 PhC-elements (**b**) 11 PhC-elements (**c**) 13 PhC-elements (**d**) 15 PhC-elements.

To investigate the optimum value of cavity-radius, it is varied for three selected values of r = 0.100*a*, 0.207*a*, and 0.350*a* for 9, 11, 13, and 15 PhC-elements. In all the considered cases, the data signal is being amplified and ω_c is being shifted when the control signal is activated. Additionally, as the cavity-radius increases, the guided modes undergo a redshift in all the cases. Figure 9a shows variation in the cavity-radius for 9 PhC elements, where the highest amplification of the data signal is observed for r = 0.10*a* and 0.207*a*. Similarly, also for the case studies with 11, 13 and 15 PhC-elements, the highest amplification is observed for cavity-radii of r = 0.10*a* and 0.207*a*. Moreover, the few numbers of PhC-elements in the structure offers lower reflection peaks and a wider linewidth, resulting in a lower quality factor of resonant modes. However, on the contrary to this, fewer number of PhC-elements show a better optical amplification and switching effect. Considering these facts, the best results for optical switching action are observed in the structure with 9 PhC-elements and cavity-radius as r = 0.10*a*. A detailed report on the numerical results of the spectral parameters in terms of differences among the different PhCs-based structures in terms of ω_c, reflection peaks, linewidth, number of PhC-elements, and cavity-radius for both excitation with data as well as control signal is provided in Table 3.

4.6. Comparative Analysis of Reflection Peak against Variation in the Number of PhC Elements for Optical Switching Action

To give a more detailed insight into the optical switching action, the values of reflection peaks are plotted against the cavity-radius for all four cases of a varying number of PhC-elements (Figure 10). The reflection peaks for a single source (the data signal) are shown in solid circles, whereas, the reflection peaks of the data signal after turning on the control signal are shown with hollow circles. All the three considered cavity-radii values are

depicted in different colors. It can be concluded from the graphical analysis that the best optical switching and amplification effect can be achieved with the device having 9 PhC-elements and cavity-radius as r = 0.10*a*.

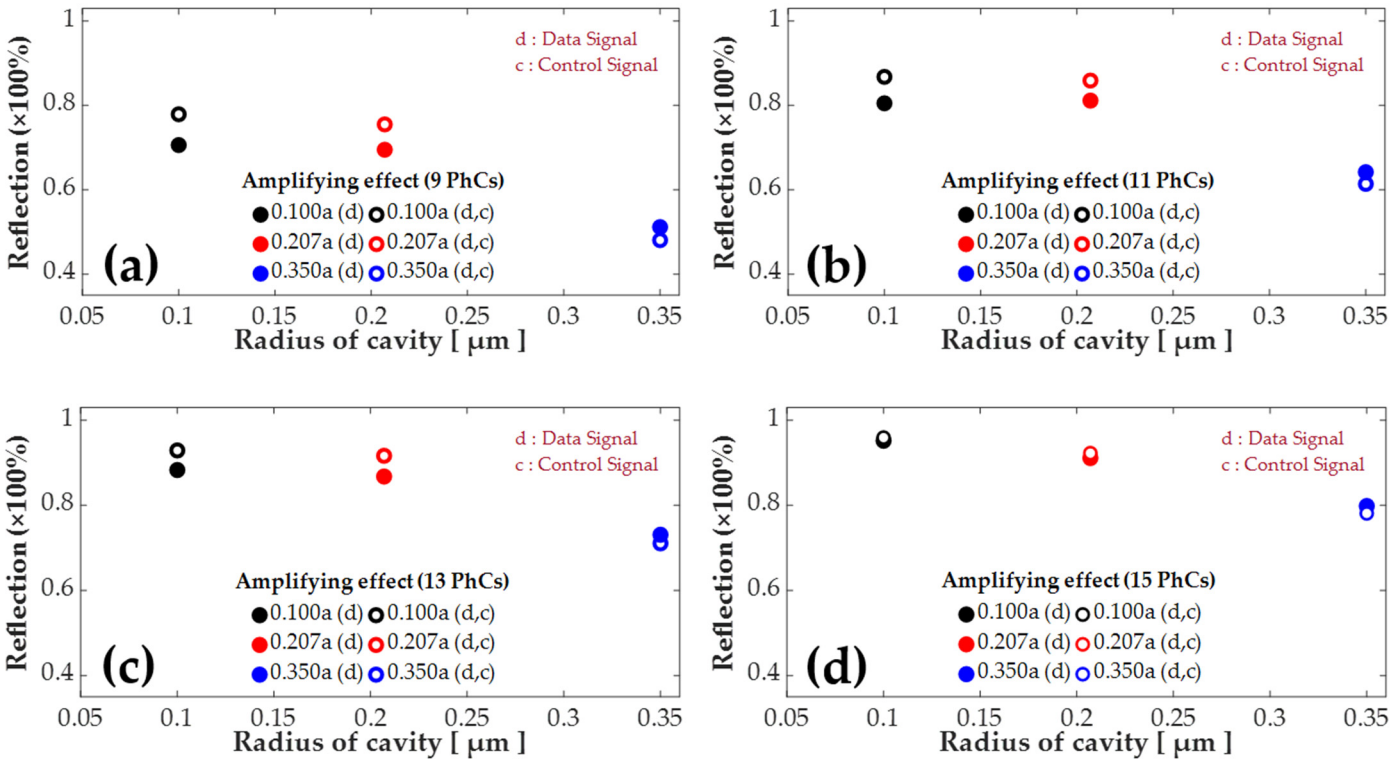

Figure 10. Reflection peaks vs the cavity-radius with single source response plotted in solid circles and dual source (data and control signal) plotted as hollow circles. (**a**) 9 PhC-elements (**b**) 11 PhC-elements (**c**) 13 PhC-elements (**d**) 15 PhC-elements.

4.7. Comparative Analysis of the Linewidth against Variation in the Number of PhC Elements for Optical Switching Action

To investigate the bandwidth and quality of the resonant modes, a comprehensive study on variation in the linewidth of the resonant modes for the change in structural parameters and implementation of the optical switching action is discussed in this section. The graphical representation of the linewidth against the cavity-radius for all of the four PhC based structures are investigated with the effects of the control signal on the output of the data signal, the approach in reflected in Figure 11a–d. For all the considered cases, the overall variation of linewidth is from 0.069 to 0.100 μm. As a generalized trend for optical switching, the linewidth of the data signal is decreased after the application of the control signal. Whereas, the minimum value of linewidth and the smallest difference of linewidth of the data signal after application of the control signal is achieved for 15 PhC-elements (Figure 11d). As explained earlier, the more the number of PhC-elements, the better the coupling and confinement of energy into the periodic structure. The case study in Figure 11a, with 9 PhC-elements offers the largest linewidth of the modes and a larger difference in linewidth of data signal without and with the application of the control signal. It can be concluded here that for better optical filtering and field confinement characteristics, a larger number of PhC-elements is preferred would yield a narrow linewidth and a better-quality factor. Whereas, for optical amplification and switching effect, a structure with lesser number of PhC-elements is preferred which would yield a broader linewidth.

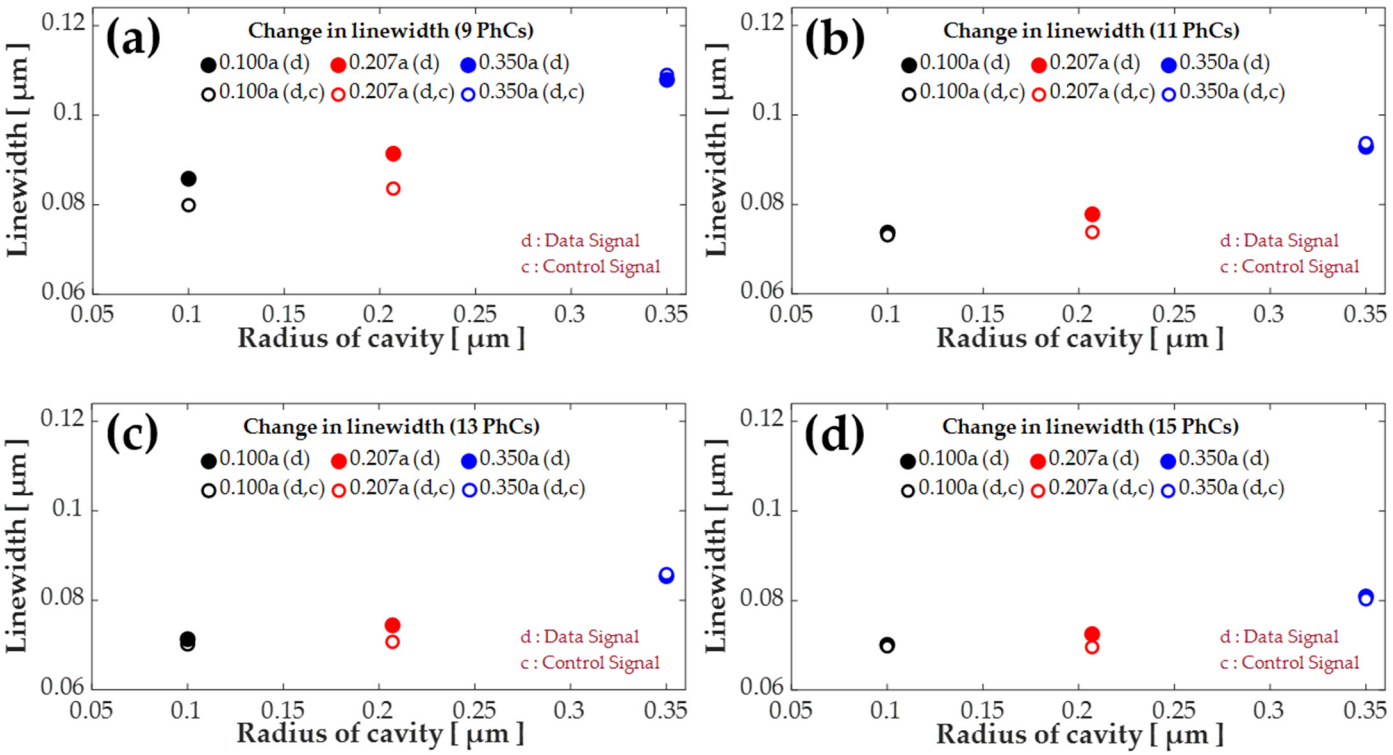

Figure 11. Variation in the linewidth of resonant modes in optical switching action for different numbers of PhC-elements and change in cavity-radius. Single source signal shown in sold circles and dual source signal with hollow circles. (**a**) 9 PhC-elements (**b**) 11 PhC-elements (**c**) 13 PhC-elements (**d**) 15 PhC-elements.

4.8. Comparative Analysis of Quality Factor against Variation in the Number of PhC Elements and Radius of PhC-Cavity for Optical Switching Action

To evaluate the spectral characteristics of the designed optical switching device, a comparative analysis of the quality factor of the resonant modes is graphically presented in Figure 12. It can be observed in all the subplots (Figure 12a–d) that the quality factor of the data signal is improved with the application of the control signal which largely justifies the device design for optical switching action. The highest quality factor is achieved for the structures with 15 PhC-elements and cavity-radius of 0.100*a* and the lowest quality factor of 9.74 is achieved for 9 PhC-elements and cavity-radius of 0.305*a*. In addition to this, the 9 PhC-elements arrangement offers the largest value of quality factor improvement in data signal when the control signal is applied which again adds to the quality of optical switching offered by the device. Summarizing, the quality factor improves to 11.87 for 11 PhC elements, 13.23 for 13 PhC-elements, and 13.80 for 15 PhC-elements. The different number of PhC-elements and cavity-radii shown in Figure 12a–d, gives the user a wide range of quality factor selection making the device suitable for different optical amplification and switching scenarios.

Table 3, gathers a detailed overview of the spectral characteristics of all the investigated PhCs structures with different numbers of PhC-elements and cavity-radii for both single and dual source action. The reported spectral characteristic includes ω_c, reflection peaks and linewidth. By analyzing these parameters, an appropriate design of the optical switch can be chosen to yield the desired spectral characteristics for a specific application.

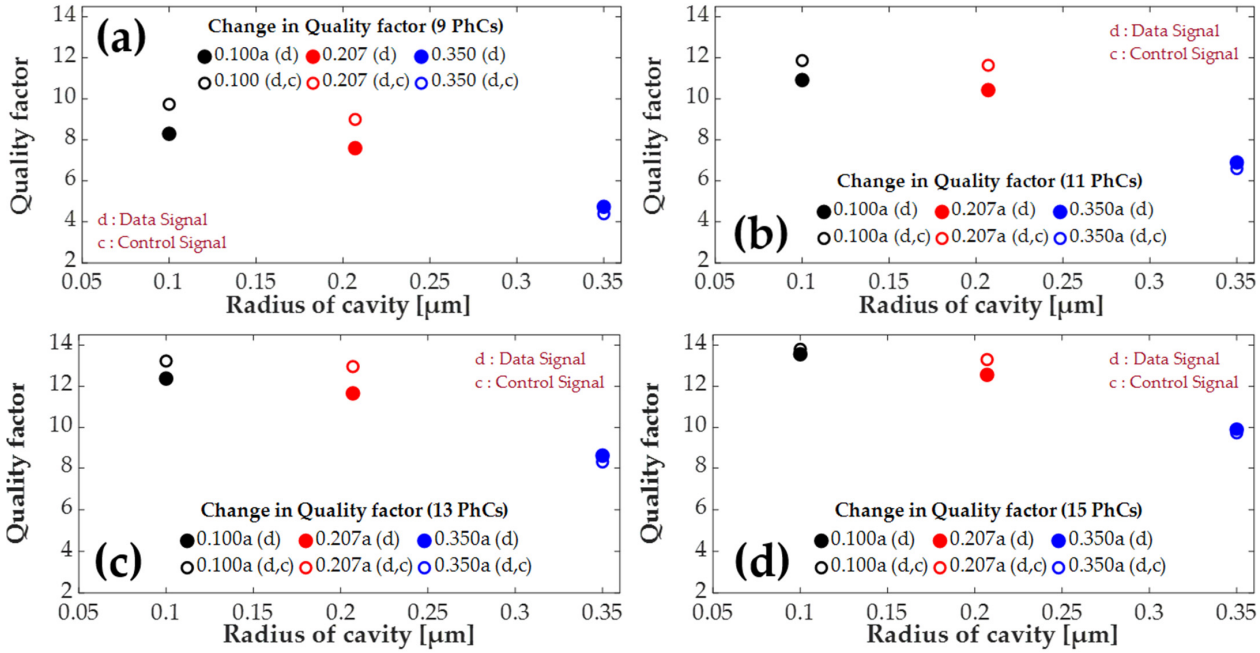

Figure 12. Quality factor of data signal before and after amplification for different number of PhC-elements and cavity-radii of 0.100a, 0.207a and 0.350a. Single source excitation is shown in solid circles and dual source action in hollow circles. (**a**) 9 PhC-elements. (**b**) 11 PhC-elements. (**c**) 13 PhC-elements. (**d**) 15 PhC-elements.

Table 3. Comparative analysis of spectral characteristics of different designs of the proposed optical switch for single (data signal) and dual source (data and control) action.

Radius of Cavity (9 PhCs)	Resonant Wavelength (μm)		Reflection Peaks (×100%)		Linewidth (μm)	
	Single Sour	Two Sources	Single Source	Two Sources	Single Source	Two Sources
0.100a	1.55	1.551	0.706	0.779	0.0858	0.0799
0.207a	1.546	1.546	0.695	0.755	0.0914	0.0836
0.350a	1.556	1.549	0.5116	0.4806	0.1079	0.1090
Radius of Cavity (11 PhCs)	**Resonant Wavelength (μm)**		**Reflection Peaks (×100%)**		**Linewidth (μm)**	
	Single Source	**Two Sources**	**Single Source**	**Two Sources**	**Single Source**	**Two Sources**
0.100a	1.549	1.55	0.805	0.8677	0.0737	0.0731
0.207a	1.545	1.545	0.8114	0.859	0.0778	0.0738
0.350a	1.55	1.547	0.6419	0.614	0.0929	0.0937
Radius of Cavity (13 PhCs)	**Resonant Wavelength (μm)**		**Reflection Peaks (×100%)**		**Linewidth (μm)**	
	Single Source	**Two Sources**	**Single Source**	**Two Sources**	**Single Source**	**Two Sources**
0.100a	1.545	1.546	0.883	0.929	0.0713	0.0702
0.207a	1.543	1.543	0.8678	0.9165	0.0744	0.0707
0.350a	1.546	1.545	0.731	0.7107	0.0854	0.0854
Radius of Cavity (15 PhCs)	**Resonant Wavelength (μm)**		**Reflection Peaks (×100%)**		**Linewidth (μm)**	
	Single Source	**Two Sources**	**Single Source**	**Two Sources**	**Single Source**	**Two Sources**
0.100a	1.542	1.544	0.9518	0.9592	0.0701	0.0697
0.207a	1.542	1.543	0.9112	0.9228	0.0725	0.0696
0.350a	1.544	1.543	0.7985	0.7811	0.0809	0.0803

5. Discussion

To validate the novelty of the proposed optical switch design, an overview of the pre-existing works which used similar structural designs and methods is provided in this section. The research work in [44] reports a 3D-FDTD simulation with elliptical PhCs arranged in a triangular lattice in silicon membrane having a centralized point-defect nanocavity used as a fluid sensor. The quality factor and resonant wavelength are tuned by changing the size of the point-defect and the number of PhCs. A higher quality factor in the range of 10^4 is reported as refractive of n = 3.42 membrane is used and the device is meant to achieve a higher sensitivity. Apart from this, another study in [45] presents a PhC-based optical switch design with a silicon waveguide deposited on the top of a SiO_2 substrate and covered with a polymer cladding. The PhCs are arranged in a triangular lattice and a line-defect cavity is designed in the middle to tune with spectral parameters. The simulations are performed in 3D-FDTD and the optical switching mechanism is implemented by changing the refractive index of the polymer cladding. Moreover, the quality factor is tuned by varying the radius of the cavity.

The above-cited works differ from the proposed work in many ways. First, both the works are based on semiconductor materials and the type of cavities used are point-defects and line-defects not a air-hole cavities as in the case of this work. Moreover, the cited works place the cavity in the middle of the structure unlike the case of this work where the cavity is placed at the start of the structure. Furthermore, Ref. [44] reports a fluid sensor, and [45] reports an optical switch that works based on wavelength switching by varying the refractive index of the cladding. This work proposes less complex structure and easy to implement optical switching mechanism by amplification of data signal with the help of a control signal, which makes the idea novel.

6. Conclusions

In this paper, a novel design of the optical switch working on the principle of GMR in PhC structure is numerically investigated. The designed structure serves a dual purpose of Fano-filtering the data signal to reduce the noise and implement an optical switching action by using a control signal. The incident data signal is coupled out-of-plane into the periodic waveguide using GMR, whereas it is optically enhanced using an in-plane index-guided control signal. The spectral properties of the data signal and optical switching action are optimized by varying the number of PhC-elements and the radius of the cavity. The number of PhC elements varied between 9 to 15 periods to tune the optical filtering and switching properties of the data signal. The PhC-cavity is introduced at the start of the lattice to help shift the center wavelength w_c and its radius is varied from $0.100a$ to $0.350a$. The investigated spectral properties include a shift in w_c, reflection peaks, quality factor, and linewidth of the data signal in the output spectrum. Considering the optical switching action, the best value of optical amplification was observed at a cavity of radius $0.100a$ despite the number of PhC-elements. It was observed that a higher number of PhC-elements (i.e., 13 and 15) yielded a better quality of signal with a narrower linewidth and a higher reflection peak but a lower number of PhC-elements (i.e., 9 and 11) provided better control of data signal in optical switching action. Therefore, the structures comprising 9 and 11 PhCs with a cavity of radius $0.100a$ is preferred for the efficient design of the optical switch. Considering optical switching action, maximum amplification of 7% is achieved with a wavelength shift of 0.001 μm and a quality factor of 11.87. The device is proposed to be used in all kinds of applications where optical amplification is required including optical switches, transistors, logical gates, optical circuits, filters, and sensors.

Author Contributions: Conceptualization, A.U.R., Y.K., M.I., M.A.B., N.L.K., S.N.K.; methodology, A.U.R., Y.K., M.I., M.A.B., N.L.K., S.N.K.; software, A.U.R., Y.K., M.I., M.A.B., N.L.K., S.N.K.; validation, A.U.R., Y.K., M.I., M.A.B., N.L.K., S.N.K.; formal analysis, A.U.R., Y.K., M.I., M.A.B., N.L.K., S.N.K.; investigation, A.U.R., Y.K., M.I., M.A.B., N.L.K., S.N.K.; resources, A.U.R., Y.K., M.I., M.A.B., N.L.K., S.N.K.; data curation, A.U.R., Y.K., M.I., M.A.B., N.L.K., S.N.K.; writing—original draft preparation, A.U.R., Y.K., M.I., M.A.B., N.L.K., S.N.K.; writing—review and editing, A.U.R., Y.K.,

M.I., M.A.B., N.L.K., S.N.K.; visualization, A.U.R., Y.K., M.I., M.A.B., N.L.K., S.N.K.; supervision, A.U.R., Y.K., M.I., M.A.B., N.L.K., S.N.K.; project administration, A.U.R., Y.K., M.I., M.A.B., N.L.K., S.N.K.; funding acquisition, M.A.B. All authors have read and agreed to the published version of the manuscript.

Funding: The research was supported by the Ministry of Science and Higher Education of the Russian Federation in the financing of new laboratories under the guidance of young scientists within the framework of the national project "Science and Universities" (project FSSS-2021-0016) in the part of numerical calculations and under the FSRC "Crystallography and Photonics" of the Russian Academy of Sciences (the state task No. 007-GZ/Ch3363/26) in the part of theoretical analysis.

Data Availability Statement: Not applicable.

Acknowledgments: The authors would like to pay gratitude to Nanophotonics Research Group (BUITEMS) and Parveen Ghoutie for their support and appreciation.

Conflicts of Interest: The authors declare no conflict of interest.

References

1. Wang, Y.; Yang, J.; Wang, Z.; Kong, X.; Sun, X.; Tian, J.; Zhang, X.; Zhao, X.; Liu, Y.; Li, H.; et al. The Development and Progression of Micro-Nano Optics. *Front. Chem.* **2022**, *10*, 916553. [CrossRef] [PubMed]
2. Demkov, A.A.; Bajaj, C.; Ekerdt, J.G.; Palmstrøm, C.J.; Ben Yoo, S.J. Materials for Emergent Sili-con-Integrated Optical Computing. *J. Appl. Phys.* **2021**, *130*, 070907. [CrossRef] [PubMed]
3. Bogaerts, W.; Pérez, D.; Capmany, J.; Miller, D.A.; Poon, J.; Englund, D.; Morichetti, F.; Melloni, A. Programmable Photonic Circuits. *Nature* **2020**, *586*, 207–216. [CrossRef] [PubMed]
4. Ji, X.; Liu, J.; He, J.; Wang, R.N.; Qiu, Z.; Riemensberger, J.; Kippenberg, T.J. Compact, Spa-tial-Mode-Interaction-Free, Ultralow-Loss, Nonlinear Photonic Integrated Circuits. *Commun. Phys.* **2022**, *5*, 84. [CrossRef]
5. Masilamani, S.; Punniakodi, S. Photonic Crystal Ring Resonator Based Optical MUX/DEMUX Design Structures: A Survey and Comparison Study. *J. Opt.* **2020**, *49*, 168–177. [CrossRef]
6. Yanik, M.F.; Fan, S.; Soljačić, M.; Joannopoulos, J.D. All-optical transistor action with bistable switching in a photonic crystal cross-waveguide geometry. *Opt. Lett.* **2003**, *28*, 2506–2508. [CrossRef]
7. Krishnamurthy, V.; Chen, Y.; Ho, S.-T. Photonic Transistor Design Principles for Switching Gain $\geq$ 2. *J. Light. Technol.* **2013**, *31*, 2086–2098. [CrossRef]
8. Butt, M.; Khonina, S.; Kazanskiy, N. Recent advances in photonic crystal optical devices: A review. *Opt. Laser Technol.* **2021**, *142*, 107265. [CrossRef]
9. Tavana, S.; Bahadori-Haghighi, S.; Sheikhi, M.H. High-performance electro-optical switch using an anisotropic graphene-based one-dimensional photonic crystal. *Opt. Express* **2022**, *30*, 9269. [CrossRef]
10. Xu, H.; Lin, Z.; Dai, X. MoTe Quantum Dots-Based All-Optical Switching. *Opt. Commun.* **2022**, *506*, 127573. [CrossRef]
11. Daghooghi, T.; Soroosh, M.; Ansari-Asl, K. Low-power all-optical switch based on slow light photonic crystal. *Photonics Netw. Commun.* **2022**, *43*, 177–184. [CrossRef]
12. Khan, Y.; Rehman, A.U.; Batool, B.A.; Noor, M.; Butt, M.A.; Kazanskiy, N.L.; Khonina, S.N. Fabrication and Investigation of Spectral Properties of a Dielectric Slab Waveguide Photonic Crystal Based Fano-Filter. *Crystals* **2022**, *12*, 226. [CrossRef]
13. Joannopoulos, J.D.; Villeneuve, P.R.; Fan, S. Photonic Crystals: Putting a new twist on Light: A Review. *Nature* **1997**, *386*, 143–149. [CrossRef]
14. Hu, X.; Gong, Q.; Liu, Y.; Cheng, B.; Zhang, D. All-optical switching of defect mode in two-dimensional nonlinear organic photonic crystals. *Appl. Phys. Lett.* **2005**, *87*, 231111. [CrossRef]
15. Khan, Y.; Butt, M.A.; Kazanskiy, N.L.; Khonina, S.N. Numerical Study of Fabrication-Related Effects of the Structural-Profile on the Performance of a Dielectric Photonic Crystal-Based Fluid Sensor. *Materials* **2022**, *15*, 3277. [CrossRef]
16. Hu, X.; Jiang, P.; Ding, C.; Yang, H.; Gong, Q. Picosecond and low-power all-optical switching based on an organic photonic-bandgap microcavity. *Nat. Photonics* **2008**, *2*, 185–189. [CrossRef]
17. Heuck, M.; Kristensen, P.T.; Elesin, Y.; Moerk, J. Improved switching using Fano resonances in photonic crystal structures. *Opt. Lett.* **2013**, *38*, 2466–2468. [CrossRef]
18. Dong, H.M.; Bang, N.H.; Khoa, D.X.; Van Doai, L. All-optical switching via spontaneously generated coherence, relative phase and incoherent pumping in a V-type three-level system. *Opt. Commun.* **2021**, *507*, 127731. [CrossRef]
19. Dhama, R.; Panahpour, A.; Pihlava, T.; Ghindani, D.; Caglayan, H. All-optical switching based on plasmon-induced Enhancement of Index of Refraction. *Nat. Commun.* **2022**, *13*, 3114. [CrossRef]
20. Rebhi, S.; Najjar, M. Hourglass Nonlinear Photonic Crystal Cavity for Ultra-Fast All-Optical Switching. *Optik* **2018**, *180*, 858–865. [CrossRef]
21. Belotti, M.; Galisteo-López, J.F.; De Angelis, S.; Galli, M.; Maksymov, I.; Andreani, L.C.; Peyrade, D.; Chen, Y. All-optical switching in 2D silicon photonic crystals with low loss waveguides and optical cavities. *Opt. Express* **2008**, *16*, 11624–11636. [CrossRef] [PubMed]

22. Pezeshki, H.; Darvish, G. Design of photonic crystal microcavity based optical switches using Fano resonance effect. *Optik* **2015**, *126*, 4202–4205. [CrossRef]
23. Zhou, H.; Qiu, C.; Jiang, X.; Zhu, Q.; He, Y.; Zhang, Y.; Su, Y.; Soref, R. Compact, submilliwatt, 2 × 2 silicon thermo-optic switch based on photonic crystal nanobeam cavities. *Photonics Res.* **2017**, *5*, 108–112. [CrossRef]
24. Granpayeh, A.; Habibiyan, H.; Parvin, P. Photonic Crystal Directional Coupler for All-Optical Switching, Tunable Multi/Demultiplexing and Beam Splitting Applications. *J. Mod. Opt.* **2018**, *66*, 359–366. [CrossRef]
25. Takiguchi, M.; Shinya, A.; Notomi, M.; Takemura, N.; Tateno, K.; Nozaki, K.; Sasaki, S.; Sergent, S.; Kuramochi, E.; Wasawo, T.; et al. All-Optical Switching using a III-V Nanowire Integrated Si Photonic Crystal Nanocavity. In Proceedings of the 2019 IEEE Photonics Conference (IPC), San Antonio, TX, USA, 29 September–3 October 2019; pp. 1–2. [CrossRef]
26. Bekele, D.A.; Marchevsky, A.; Saudan, Q.; Yu, Y.; Galili, M.; Oxenlowe, L.K.; Yvind, K.; Mork, J. Towards High-Speed Fano Photonic Switches. In Proceedings of the 2019 21st International Conference on Transparent Optical Networks (ICTON), Angers, France, 9–13 July 2019; pp. 1–4. [CrossRef]
27. Zhang, X.; Yang, J. Ultrafast Plasmonic Optical Switching Structures and Devices. *Front. Phys.* **2019**, *7*, 190. [CrossRef]
28. Azizpour, M.R.J.; Soroosh, M.; Dalvand, N.; Seifi-Kavian, Y. All-Optical Ultra-Fast Graphene-Photonic Crystal Switch. *Crystals* **2019**, *9*, 461. [CrossRef]
29. Rutckaia, V.; Schilling, J. Ultrafast low-energy all-optical switching. *Nat. Photonics* **2019**, *14*, 4–6. [CrossRef]
30. Eid, M.M.; Rashed, A.N.Z. High speed optical switching gain based EDFA model with 30 Gb/s NRZ modulation code in optical systems. *J. Opt. Commun.* **2020**, 1–6. [CrossRef]
31. Kuttruff, J.; Garoli, D.; Allerbeck, J.; Krahne, R.; De Luca, A.; Brida, D.; Caligiuri, V.; Maccaferri, N. Ultrafast all-optical switching enabled by epsilon-near-zero-tailored absorption in metal-insulator nanocavities. *Commun. Phys.* **2020**, *3*, 114. [CrossRef]
32. Nguyen, H.A.; Grange, T.; Malik, N.S.; Dupuy, E.; Tumanov, D.; de Assis, P.L.; Yeo, I.; Fratini, F.; Gregersen, N.; Auffèves, A.; et al. Ultra-Low Power Optical Transistor Using a Single Quantum Dot. In Proceedings of 2017 Conference on Lasers and Electro-Optics Europe & European Quantum Electronics Conference (CLEO/Europe-EQEC), Munich, Germany, 25–29 June 2017.
33. Goodarzi, A.; Ghanaatshoar, M. Coherent all-optical transistor based on frustrated total internal reflection. *Sci. Rep.* **2018**, *8*, 5069. [CrossRef]
34. Moradi, M.; Mohammadi, M.; Olyaee, S.; Seifouri, M. Design and Simulation of a Fast All-Optical Modulator Based on Photonic Crystal Using Ring Resonators. *Silicon* **2021**, *14*, 765–771. [CrossRef]
35. Rani, P.; Kalra, Y.; Sinha, R. Design of all optical logic gates in photonic crystal waveguides. *Optik* **2015**, *126*, 950–955. [CrossRef]
36. Goudarzi, K.; Mir, A.; Chaharmahali, I.; Goudarzi, D. All-optical XOR and OR logic gates based on line and point defects in 2-D photonic crystal. *Opt. Laser Technol.* **2016**, *78*, 139–142. [CrossRef]
37. Younis, R.M.; Areed, N.F.F.; Obayya, S.S.A. Fully Integrated AND and OR Optical Logic Gates. *IEEE Photonics Technol. Lett.* **2014**, *26*, 1900–1903. [CrossRef]
38. Mondal, H.; Goswami, K.; Sen, M.; Khan, W.R. Design and Analysis of All Optical Logic NOR Gate Based on Linear Optics. *Opt. Quantum Electron.* **2022**, *272*, 272. [CrossRef]
39. Sharma, A.; Goswami, K.; Mondal, H.; Datta, T.; Sen, M. A review on photonic crystal based all-optical logic decoder: Linear and nonlinear perspectives. *Opt. Quantum Electron.* **2022**, *54*, 90. [CrossRef]
40. Saudan, Q.; Bekele, D.A.; Dong, G.; Yu, Y.; Yvind, K.; Mørk, J.; Galili, M. Crosstalk-free all-optical switching enabled by Fano resonance in a multi-mode photonic crystal nanocavity. *Opt. Express* **2022**, *30*, 7457. [CrossRef]
41. Khan, Y. Design and Numerical Simulation of Dielectric Photonic Crystal Devices and Investigation of an Optical Charac-terization Method. Ph.D Thesis, University of Kassel, Kassel, Germany, 2017.
42. MEEP Tutorial. Available online: http://ab-initio.mit.edu/wiki/index.php/Meep_tutorial (accessed on 15 June 2022).
43. Oskooi, A.F.; Roundy, D.; Ibanescu, M.; Bermel, P.; Joannopoulos, J.D.; Johnson, S.G. Meep: A Fexible Free-Software Package for Electromagnetic Simulations by the FDTD Method. *Comput. Phys. Commun.* **2010**, *181*, 687–702. [CrossRef]
44. Kassa-Baghdouche, L. Optical properties of a point-defect nanocavity-based elliptical-hole photonic crystal for mid-infrared liquid sensing. *Phys. Scr.* **2019**, *95*, 015502. [CrossRef]
45. Kassa-Baghdouche, L.; Boumaza, T.; Bouchemat, M. Optimization of *Q*-factor in nonlinear planar photonic crystal nanocavity incorporating hybrid silicon/polymer material. *Phys. Scr.* **2015**, *90*, 065504. [CrossRef]